J. Fluid Mech. (1993), *vol.* 250, *pp.* 669–687

The propagation of intrusion fronts of high density ratios

By H. P. GRÖBELBAUER[1], T. K. FANNELØP[1] AND R. E. BRITTER[2]

[1] Institute of Fluid Dynamics, Swiss Federal Institute of Technology, Zürich, Switzerland

[2] Department of Engineering, University of Cambridge, Cambridge CB2 1P2, UK

(Received 25 March 1992 and in revised form 7 December 1992)

The propagation of gravity fronts of high density ratios has been studied experimentally (exchange flow) and by computer simulation. Non-Boussinesq fronts are known to occur in certain safety problems (chemical spills and fires), and we have investigated seven gas combinations giving density ratios from near unity to well over 20. The results are presented in terms of a density parameter ρ^* which remains finite both in the weak ($\rho^* = 0$) and the strong ($\rho^* = 1$) limit. The front velocities, measured by means of hot wires, are found to fall on two distinct curves, one for the slower light-gas fronts and one for the faster heavy-gas fronts. Two fractional depths, $\Phi = \frac{1}{2}$ (lock exchange) and $\Phi = \frac{1}{6}$, have been investigated in detail and results for the interesting case $\Phi \to 0$ have been obtained by extrapolation. To aid in the extrapolation and for comparison, all experimental (and some intermediate) cases have been simulated by means of a general purpose CFD-code (PHOENICS). Good agreement is found for cases without convergence problems, i.e. for heavy-gas fronts of density ratio less than 5. Further information on frontal shape etc. has been obtained from visualization. The extrapolations to infinite depth indicate a limiting speed for both the heavy- and light-gas fronts close to the values predicted from shallow-layer theory for the analogous dam-break problem.

1. Introduction

The propagation of intrusion fronts is a topic of prime interest in geophysics and hydraulics, most often in connection with gravity currents and lock-exchange problems. A general review will be found in the recent book by Simpson (1987) and one for research on dense-gas fronts in Britter (1989). In certain applications concerned with safety, the density ratio across the front can be rather high, and the usual relation for the front velocity appears to give unreasonable results. On denoting the densities of the heavy and light fluids with indices 2 and 1 respectively, the thickness of the intruding layer h and the acceleration due to gravity g, the relation usually specified is

$$u_F = k\left(gh\frac{\rho_2-\rho_1}{\rho_1}\right)^{\frac{1}{2}} \quad \text{or} \quad u_F = k(g'h)^{\frac{1}{2}} \tag{1a}$$

using common nomenclature. The controversial point relates to the use of ρ_1 in the denominator. For most natural flows the density difference is so small that it does not matter much. But for accidental releases of hazardous gases that are heavier than air,

in common use in the chemical process industries, a density ratio of 2 to 5 would be of interest. In that case the use of g' or the alternative g'' defined by

$$g'' = g\frac{\rho_2 - \rho_1}{\rho_2}$$

leads to quite different results. Fay (1982) has drawn attention to this controversy as 'one of the unresolved problems in heavy gas dispersion'. He has pointed out that the use of g' can lead to an acceleration exceeding g for high (but not unusual) density ratios, clearly an unreasonable result.

High density ratios can occur, not only for accidental releases of industrial gases but also for the spreading of hot fire gases under ceilings, another safety problem. The easiest way to produce a front of high density ratio would be to release a light gas such as helium under a ceiling. In air this would produce an intrusion front of density ratio 7, sufficient to indicate which alternative, g' or g'', would give better prediction. Already the Thorney Island heavy-gas experiments (1982–83) have used density ratios in excess of four (Freon 12 in air, McQuaid 1985). But the high-aspect-ratio release produced so much mixing in the initial slumping process prior to the establishment of a clear density front that it is difficult to draw a firm conclusion from the data.

It appears that the data available prior to 1991 on the propagation of density fronts on level surfaces pertain only to flows of low density ratio for which the Boussinesq approximation is applicable. (An exception would be snow avalanches and other two-phase flows down slopes, but here many additional parameters would be of importance.) Most experiments so far have been performed with liquids, usually water and salt-in-water solutions. For such fluids a high density ratio cannot be easily produced and this is perhaps why the controversy associated with the frontal condition has not been settled.

Recent research on chemical process safety has focused on accidental gas releases, both single- and two-phase (vapour/droplet) flows. To obtain information applicable to such problems, we have tried to produce moving fronts of very high density ratio by releasing gases of widely different densities in a large gas-tight closed volume (a rectangular channel). In an open room we can attain, as noted, only a ratio of 7 (helium/air) or 4 (Freon 12/air) at moderate cost and in safety. The most exotic (and expensive) Freon derivative, i.e. Freon RC 318, is seven times heavier than air. Releases of hydrogen in air would produce an even higher density ratio (about 14), but its use appears too hazardous in practice.

The present approach produces a maximum density ratio in excess of 20 when the environmentally benign Freon R22 is released in helium inside a closed volume, and it allows a wide range of density ratios to be studied between this limit and the low values for which the Boussinesq approximation holds. The drawback is that the set-up produces an exchange flow rather than an unbounded gravity intrusion. A simple relationship between these flows exists only for small density differences.

2. Theoretical considerations

2.1. *The different interpretations of the frontal condition*

The simplest idea is that the motion of the intrusion front is driven by the excess hydrostatic pressure and resisted by the increased pressure over the frontal region of the body formed when the intruding fluid is considered enveloped by an impermeable rounded shape. The excess hydrostatic pressure in the head is $(\rho_2 - \rho_1)gh$ whereas the

opposing stagnation pressure is $\frac{1}{2}\rho_1 u^2$. For similar flows we would expect a constant ratio between these pressures so that

$$\frac{(\rho_2-\rho_1)gh}{\frac{1}{2}\rho_1 u_F^2} = \text{const} \quad \text{or} \quad u_F = k\left(\frac{gh(\rho_2-\rho_1)}{\rho_1}\right)^{\frac{1}{2}}, \tag{1b}$$

as already indicated in (1*a*).

On assuming these pressures to be equal, a more speculative assumption for real flows, the constant k becomes $\sqrt{2}$, the same result as that obtained on using the Bernoulli equation along the dividing streamline.

To derive the frontal velocity for the lock-exchange problem, it is usual to assume that energy is conserved and that the flow is symmetric. (The latter assumption is clearly not fulfilled in the flow photographs published; e.g. in Simpson 1987.) The result obtained (see Yih 1965) is simply

$$u_F = \left(\frac{gh(\rho_2-\rho_1)}{\rho_2+\rho_1}\right)^{\frac{1}{2}}. \tag{2a}$$

By making use of the Boussinesq assumption, $\rho_2+\rho_1 \approx 2\rho_1$, we obtain one half the value of the gravity current. To put it differently: in the limit of small density differences, the two fronts move away from one another at the speed of a gravity current evaluated using the loss-free (Bernoulli) value of the constant k. But we can also make another interpretation. On rewriting the relative frontal velocity as

$$u_F = \frac{1}{\sqrt{2}}\left(\frac{gh(\rho_2-\rho_1)}{\frac{1}{2}(\rho_2+\rho_1)}\right)^{\frac{1}{2}} \tag{2b}$$

the result can be seen to depend on the mean value of the densities ρ_2 and ρ_1, reflecting the importance of the inertia of both fluids.

A third and rather different interpretation of the frontal condition is obtained when the motion of the heavy (or intruding) fluid is considered on the basis of shallow-layer theory. From the relevant equations for this layer, one can deduce a characteristic wave speed

$$u_W = \left(\frac{gh(\rho_2-\rho_1)}{\rho_2}\right)^{\frac{1}{2}}, \tag{3}$$

as shown by Fanneløp & Jacobsen (1983). Analytic (similarity) as well as numerical solutions of the shallow-layer equations for instantaneous releases show that once the whole layer is set in motion, the largest layer depth occurs at the front. A front with velocity u_W, will not be overtaken by disturbances within the layer, and a frontal condition of form (3) leads to a consistent formulation. Solutions analogous to those of interest for high-density-ratio fluid fronts, are known from the theory of spreading oil slicks (Fay 1969; Fanneløp & Waldman 1971). The spread is here driven by gravity and resisted by the inertia in the layer. In contrast, the flow model which is the basis for (1), implies a motion driven by gravity but resisted by external drag; the inertia of the moving layer is not considered. All three alternatives, (1), (2) and (3), are loss free in the sense of mechanical energy conservation, and possible losses (mixing, wave breaking, dissipation) are usually accounted for by adjusting the factor k in accord with experimental results.

In the literature it is often implied (but not always clearly expressed) that the intrusions of a heavy fluid on the floor or of a light fluid under the ceiling represent not only analogous flows but in reality identical flow problems. This could be true for small density differences (although many flow photographs indicate otherwise), but it is definitely not true for non-Boussinesq fronts. This can be verified by considering the

upper limits in frontal speed possible for the two types of flows. The most extreme case of a light fluid intruding under a ceiling would be the case considered by Benjamin (1968), i.e. finite external density and zero density in the intruding cavity. Expressed in terms of Froude number, the limit velocity would be

$$Fr = \frac{u_F}{(gh)^{\frac{1}{2}}} = \frac{1}{\sqrt{2}}, \tag{4}$$

where u_F is the front velocity and h the half-depth of the rectangular channel. (For other geometries analogous results are obtained.)

For a heavy fluid spreading on the floor, the most extreme case would be a fluid of finite density spreading in vacuum. There would be no external resistance, and the front velocity would depend on how fast energy can be extracted from the initial configuration. This rate is limited by the wave velocity in the (shallow) layer, and the corresponding solution is known as 'the breaking of a dam' (Stoker 1957 or Henderson 1966). In terms of Froude number this solution can be written as

$$Fr = \frac{u_F}{(gh)^{\frac{1}{2}}} = 2\sqrt{2} \tag{5}$$

and it is seen to be four times higher than the light-fluid limit for the same geometry. It is interesting to note that the expression for the front velocity given by (2) gives the correct form of the frontal velocity in all three limits considered, for weak as well as strong fronts. We will henceforth attempt a correlation of our experimental results for non-Boussinesq fronts in terms of ρ^* *vs.* Froude number where

$$\rho^* = \left(\frac{\rho_2 - \rho_1}{\rho_2 + \rho_1}\right)^{\frac{1}{2}}, \quad Fr = \frac{u_F}{(gh)^{\frac{1}{2}}}. \tag{6a, b}$$

(We note that the parameter ρ^* also occurs in Lamb's (1945, p. 370) equation for the wave speed at the common interface between two fluids of different densities, in the limit of infinite layer depth.) The discussion so far assumes constant density in both fluids. For miscible fluids and not too low Reynolds numbers there will be mixing so that the intruding flow is stratified. For an intrusion under a ceiling the density increases downward, due to mixing. The excess hydrostatic pressure, which drives the flow, has its maximum value at the ceiling where the inner density is lowest. As a result the upper layers move faster than the lower denser layers, and we observe an elongated wedge-like head. For the intrusion of a heavy fluid both the density and the excess hydrostatic pressure have their highest values near the floor, and we observe the blunt gravity current familiar from many experiments. These differences in frontal shape are most pronounced for strong fronts. (Propagating density fronts can also be produced using immiscible fluids with very different properties, density as well as viscosity and surface tension. Without mixing and with little or no internal circulation, the fronts can exhibit shapes rather different from those discussed.) The shallow-layer assumption is naturally suspect in the frontal region, in particular for the blunt fronts associated with an intruding heavy fluid. The front can under certain conditions develop into a strong vortex. Most observations of an organized vortex motion pertain to heavy-gas fronts (where spinup occurs more easily than for the denser liquids), and for relatively large density differences or for releases with initially high potential energy. It is not possible at present to state when a vortex will develop, but once present it will induce a forward velocity independent of the density ratio across the front (Britter 1989).

It is remarkable that, after many years with no apparent activity, in late 1991 two papers on non-Boussinesq fronts appeared. Our own contribution (Kunsch *et al.* 1991) proposed a unifying correlation for light- and heavy-gas fronts in terms of ρ^* with recommendations for its use in safety problems, but in this review of heavy-gas research at ETH no details were given. As the present paper with a more detailed exposition was prepared for publication, the new study of Keller & Chyou (1991, referred to herein as K&C) appeared. It includes, in addition to experiments with fronts of high density ratios, primarily liquids, a mathematical analysis of the internal hydraulics of the lock-exchange problem. K&C are mainly concerned with the hydraulics of internal flows, e.g. the case of a perfect fluid of constant density driving another fluid of different density through a closed horizontal channel. For their experimental work they made use of a very small channel (40×40 mm^2 and length 500 mm), which allowed visualization of the complete flow field, but the set-up also limited the accuracy of the front-velocity measurements, in particular for gas-in-gas intrusions. By judicious choice of fluids, K&C obtained density ratios as high as 3.3. In addition they combined the gases SF_6 and air (density ratio 5) and SF_6 and helium (density ratio 36) but they did not report any velocity data for heavy-gas fronts. The problem of particular interest to them was the purging of a liquid fuel line by means of pressurized air. In contrast, our main interest lies in the large-scale turbulent fronts found in certain safety problems as well as in many geophysical flows. To simulate such flows, we have chosen the largest scale possible. The use of exotic and expensive gases limits the practical volume of the test channel, but the volume chosen (10^3 times that of K&C) is believed sufficient to produce the flow features typical of turbulent fronts. The results presented herein give new information on the full range of gas intrusions, heavy as well as light, for lock-exchange flows. In addition we present data and information on the case of primary interest to us, i.e. the motion of strong fronts in an ambient of unlimited depth.

3. Experiments

The experiments include both a series of lock-exchange flows with gases of different densities in a closed channel of square cross-section, and a complementary series of exchange flows where the fractional depths of the counter-flowing currents are reduced to one-third of that for the classical lock-exchange flow. It was hoped that this second series would allow an extrapolation to the case of prime interest in applications, when the depth of the intrusion is much smaller than that of the ambient.

The experimental set-up is illustrated in figure 1 (*a*, *b*). A closed spreading channel of cross-section 0.3×0.3 m^2 and total length of either 3.8 or 4.5 m is divided into chambers of unequal size separated by a quick-opening gate. (Only one side could be fully instrumented. The unsymmetrical set-up reduces the volume of gas required, as gas represents a major cost item.) The chamber lengths are 3.0 and 0.8 m (or 1.5 m) respectively. The chambers were filled with gases of different densities, and to this end they were equipped with valves at the endwalls. A gas heavier than air was supplied through the low valve and air let out through the top valve, and vice versa for gases lighter than air. The concentration of gas in the chambers was monitored during the filling process and prior to a test it would be above 95% for the large chamber and above 97% for the smaller chamber. This introduces a maximum error in ρ^* (the correlation variable) of less than 1% relative to the nominal value. A higher purity would have led to considerable loss of gas and to higher cost without substantial improvement in the results obtained. It was necessary also to monitor the temperature

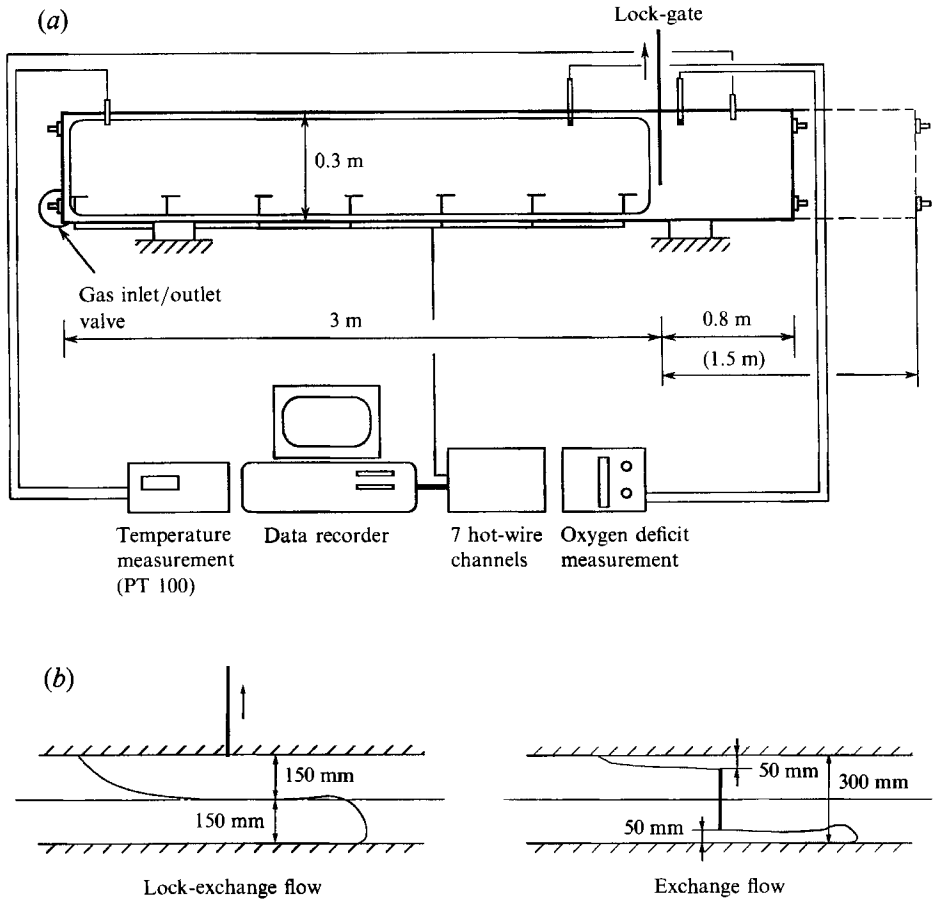

FIGURE 1. (*a*) Experimental arrangement. (*b*) Gate geometries.

drop associated with the expansion from bottle pressure to the atmospheric value. Prior to a test the temperature difference, relative to the ambient, was always less than 2 °C for the results reported herein.

The manually opened gate was suspected at first to be a major contributor to experimental scatter. But the time required to open the gate was very short in comparison with the characteristic flow times for the moving gas and the experiments showed good repeatability. (Gate velocity: 3–4 m/s, flow velocity: 0.2–1.8 m/s.) The velocity of the moving front was measured by means of seven hot-wire probes placed along the floor (heavy-gas front) or along the ceiling (light-gas front) of the larger chamber. These probes were used only as 'trip wires' to give the time of arrival of the density front.

The front panel of the larger chamber was made of transparent material to allow visualization. Of particular interest were, in addition to observations of the moving fronts, the depths of the moving layers. Some initial visualization trials were made using smoke from commercial smoke pellets. These pellets, however, generated smoke by burning and the heat released changed the density distribution. A second method based on the evaporation of oil from a vertical wire, suddenly heated by a timed electrical pulse, proved more successful (Batill & Mueller 1981). A drawback of the rather large experimental scale is that only one front and part of the opposing flow are visible in a single exposure. But it is apparent from the photos obtained that the flow

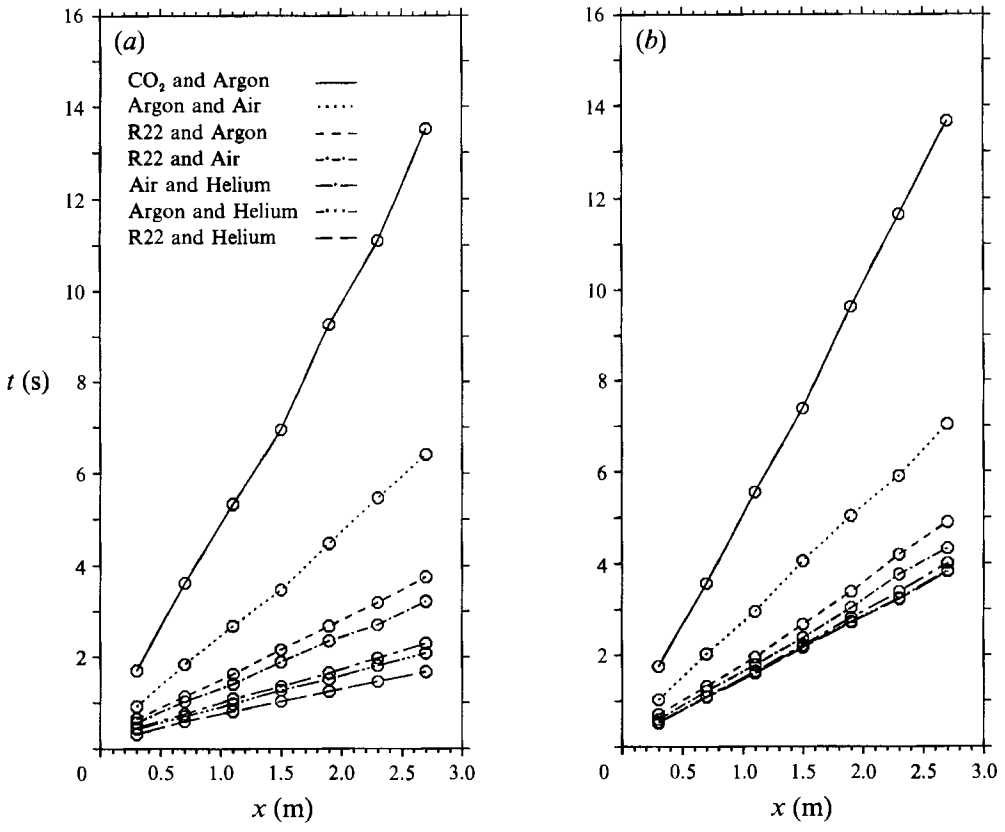

FIGURE 2. Propagation velocity of (*a*) dense-gas and (*b*) light-gas intrusion fronts.

Gases	Density ratio $r = \rho_2/\rho_1$	$\rho^* = \left(\frac{\rho_2-\rho_1}{\rho_2+\rho_1}\right)^{\frac{1}{2}}$
CO_2/Argon	1.11	0.22
Argon/Air	1.38	0.40
R22/Argon	2.18	0.61
R22/Air	2.99	0.71
Air/Helium	7.23	0.87
Argon/Helium	9.93	0.90
R22/Helium	21.6	0.95

TABLE 1. Gas combinations used for lock-exchange and exchange-flow experiments

is not symmetric and that the light-gas fronts are less blunt and appear more stable than the heavy-gas fronts, for the same density ratio. Tests were conducted with combinations of five different gases: air, argon, carbon dioxide, Freon 22 and helium, producing nominal density ratios from 1.11 (carbon dioxide in argon) to 21.6 (R22 in helium). An overview is given in table 1. Each gas combination was tested in two configurations: first with the heavy gas in the smaller chamber and the light gas in the larger and then vice versa.

(a)

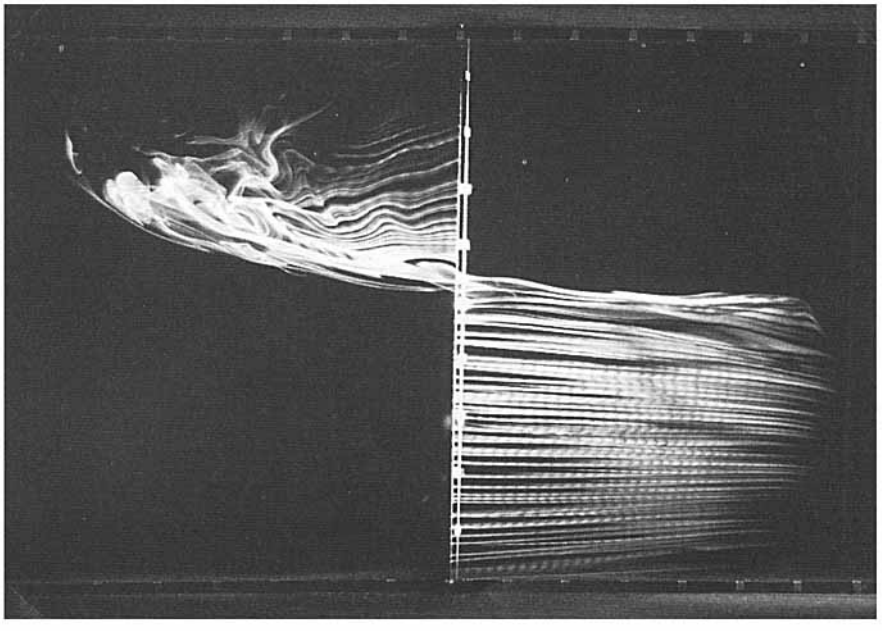

(b)

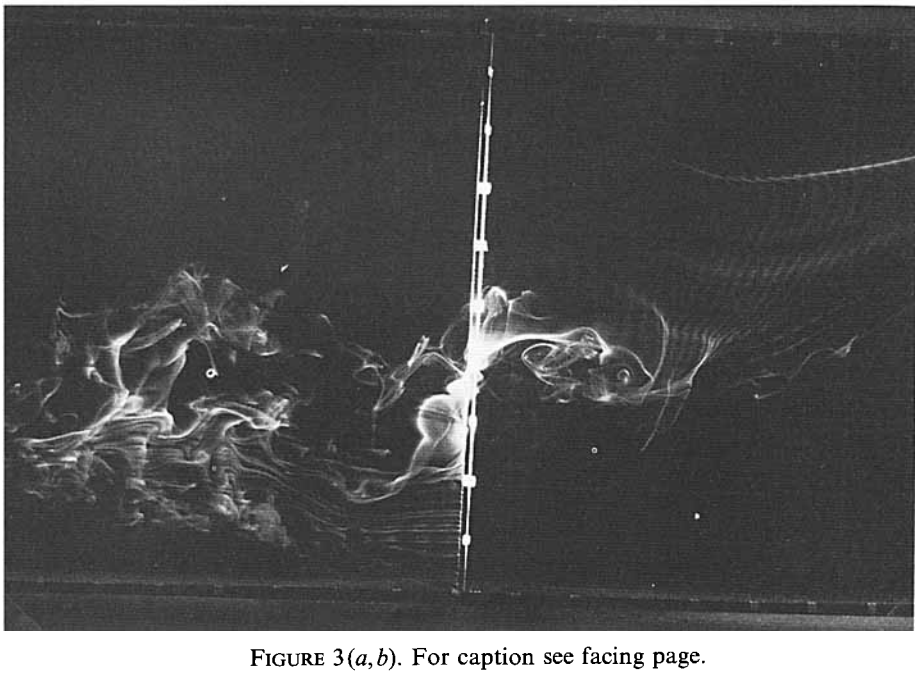

FIGURE 3(a, b). For caption see facing page.

(*c*)

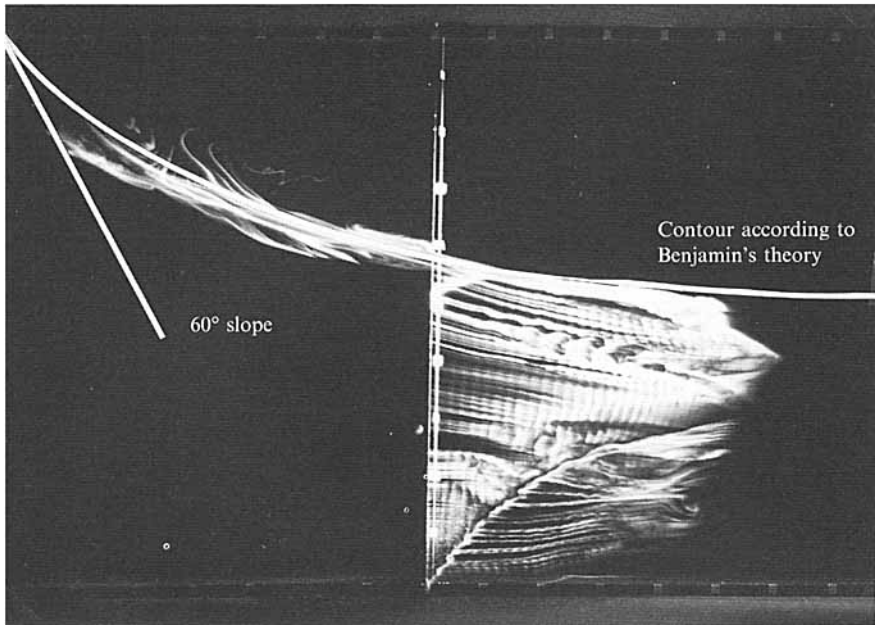

FIGURE 3. Visualization by smoke-wire technique: (*a*) helium intrusion in air, lock-exchange experiment; (*b*) air intrusion in helium, lock-exchange experiment; (*c*) helium intrusion in R22, lock-exchange experiment.

3.1. *Lock-exchange experiments*

For the smallest density ratio $\rho_2/\rho_1 = 1.11$, the Boussinesq approximation should be applicable and we would expect near identical results for light- and dense-gas fronts. Increasing differences would be expected for the six other gas combinations investigated, with density ratios up to 21.6. In figure 2 (*a*, *b*) the measured time *vs.* distance for the propagating fronts are shown. In the trial with R22 in argon ($\rho_2/\rho_1 = 2.18$) a significant difference between the fronts is observed and the dense-gas front has the higher velocity, as expected. The difference is most pronounced for the combination helium and R22 giving a speed ratio in excess of 2. The distance *vs.* time curves are remarkably linear with good repeatability and little scatter in comparison with known experimental results obtained with liquids. The electronic (hot-wire) detection of the front appears more accurate than the optical tracking of dyed fluid fronts, used in previous investigations. Turbulent fronts have certain non-uniformities (clefts and overhangs) which would be expected to show up in the velocity measurements in the form of slight irregularities. The linearity of the (x, t)-curves also indicates that the viscous effects are small and that the endwalls have little or no influence on the results. The latter point is verified further by the fact that a reversal of the flow directions had no apparent effect on the results. The effect of the initial acceleration and the finite gate-opening time are apparent only in the region upstream of the first measurement station. An exception is the case with the highest density ratio where the dense front appears to accelerate between the first and second station also. (The speed measurements used in our correlations represent data only in the linear range.)

Additional information on the flow comes from visualization. Figure 3 (*a*) shows the flow streaks originating from the smoke wire for a helium intrusion into air, initially

at rest. The limits of the wedge-shaped intrusion as well as the opposing air flow are clearly seen. There appears to be little mixing. The faster-moving air intrusion into helium at rest (figure 3*b*) appears more rounded, as expected. The streaklines indicate a more turbulent structure than in the case of the light-gas front and possibly also a dissipative jump. The elongated shape of the light-gas front is even more pronounced at higher density ratios. Figure 3(*c*) shows a helium intrusion into Freon R22. Superimposed are the theoretical frontal slope (60°) as predicted by von Karman (1940) and the complete contour of the interface according to the theory of Benjamin (1968) for cavity flow. The agreement is reasonable in view of the fact that the picture shows streaklines, as noted, and not instantaneous streamlines.

3.2. *Exchange-flow experiments*

The set-up for the exchange-flow experiments differed in two ways from those discussed. The barrier separating the two gases was divided into a fixed central part and two moving gates which opened only partially, leaving gaps of 50 mm above the floor and under the ceiling of the channel (figure 1*b*). When rebuilding the gate section, we also extended the short chamber from 0.8 to 1.5 m in length with no change in cross-section. The mechanical coupling between the upper and lower moving gates guaranteed equal opening time and speed. The velocity measurements produced results analogous to those for lock-exchange flows, but with more scatter. We attribute this to viscous effects as the boundary-layer thickness relative to the layer depth is increased by a factor of three in comparison with the lock-exchange case. Flow visualizations of the region near the gate did not give evidence of any jump phenomenon; the gravity intrusion showed near constant height with a raised head due to local mixing. As the excess hydrostatic head is not influenced by vertical mixing, we have used the unmixed fluids and the geometric height in our correlations, i.e. $(\rho_2-\rho_1)gh$.

4. Numerical calculations

All cases investigated have been studied also by means of the general purpose CFD-code PHOENICS. This code is widely used and available at major universities and research institutions (Rosten & Spalding 1987). The boundary and initial conditions are simple and well defined for numerical calculations, but the turbulence and mixing characteristics are perhaps less suitable for a general-purpose code. Inasmuch as mixing, turbulent entrainment and other loss processes are of secondary importance in our case, we have made use of the default procedure for the mass exchange input specification. The rate of mass transfer across the cell boundaries is here given as $C\rho_1 n_1 n_2 V$ (kg/s), where n_i are the volumetric fractions of species i, ρ_1 and V the cell density and volume respectively. To neglect mass transfer by letting $C = 0$ would be acceptable for the purpose of the present invetigations, but it leads to serious convergence problems. The value $C = 100$ has been used in all our calculations. (Converged solutions could not be obtained for C smaller than this value.) To 'optimize' the value of C in comparison with our experimental results was not practical in view of the very long computing time required for each case (up to 200 minutes of CPU-time on a Cyber CDC 932).

The convergence problem also required a finite amount of gas of both species to be present initially in both chambers; we have specified 99.9 % of the major and 0.1 % of the minor constituent. Turbulence was modelled by means of the standard k–ϵ procedure with a logarithmic wall function to account for the boundary layer. In the specification of the turbulent viscosity, $\nu_t = c_\mu c_D k^2/\epsilon$, the coefficients used were

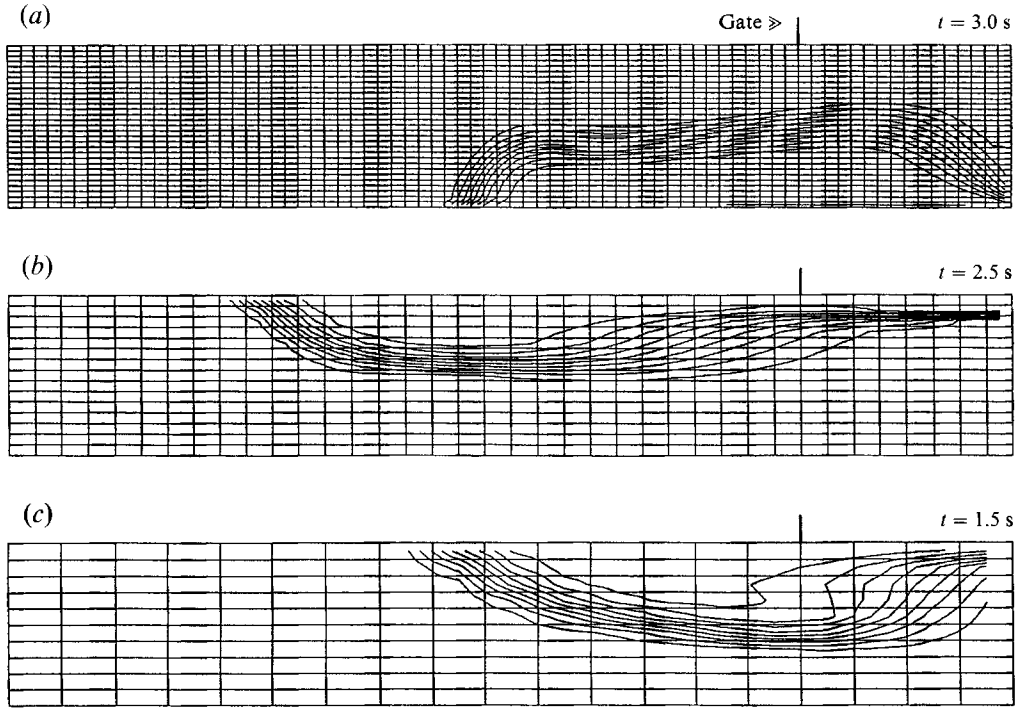

FIGURE 4. Isoconcentration lines for lock-exchange flow: (*a*) argon front in air, calculation grid, 76×30 cells; (*b*) helium front in argon, calculation grid, 38×15 cells; (*c*) helium front in R22, calculation grid, 19×10 cells.

$c_\mu = 0.5478$ and $c_D = 0.1643$ as proposed by the program developers. Three grid sizes were tried: a fine grid with 76×30 cells giving a spatial resolution of 0.05 m (x-direction) and 0.01 m (y-direction), a medium size grid of 38×15 cells and a coarse grid with only 19×10 cells. The coarse grid was needed to obtain convergence for the highest density ratio. Figure 4(*a–c*) shows the results obtained for the lock-exchange flows. (The contours shown represent the 10% isoconcentration lines.) At the times shown, the right-running fronts have been reflected from the endwall of the smaller chamber, so that only the left-running fronts are comparable with those expected in a lock-exchange experiment. The increasing elongation of the wedge-shaped light-gas front with higher density ratios appears to be confirmed by the calculation, which also shows the heavy-gas fronts to be more rounded. The front velocity is also rather well predicted for the light-gas fronts over the complete range of density ratios, whereas the predictions for the heavy-gas fronts break down for $\rho^* > 0.6$, as seen in figure 8†. Quite similar results are obtained for the exchange flows, as shown in figure 5(*a–c*). Species diffusion doubles the height of the intruding layer, as seen in figure 5, but this does not reduce the excess hydrostatic pressure and therefore does not affect the frontal speed. The velocity prediction appears to be more reliable than other quantities and features of the internal flow structure calculated by this numerical code.

† The code is primarily intended for diffusion problems, whereas the heavy-gas intrusion flows for large values of ρ^* are increasingly dominated by wave processes. A comparison between the interfacial wave speed, calculated from Lamb (1945, p. 370), and the frontal speed (experiments) show that they are nearly equal at $\rho^* \approx 0.7$ (lock-exchange case).

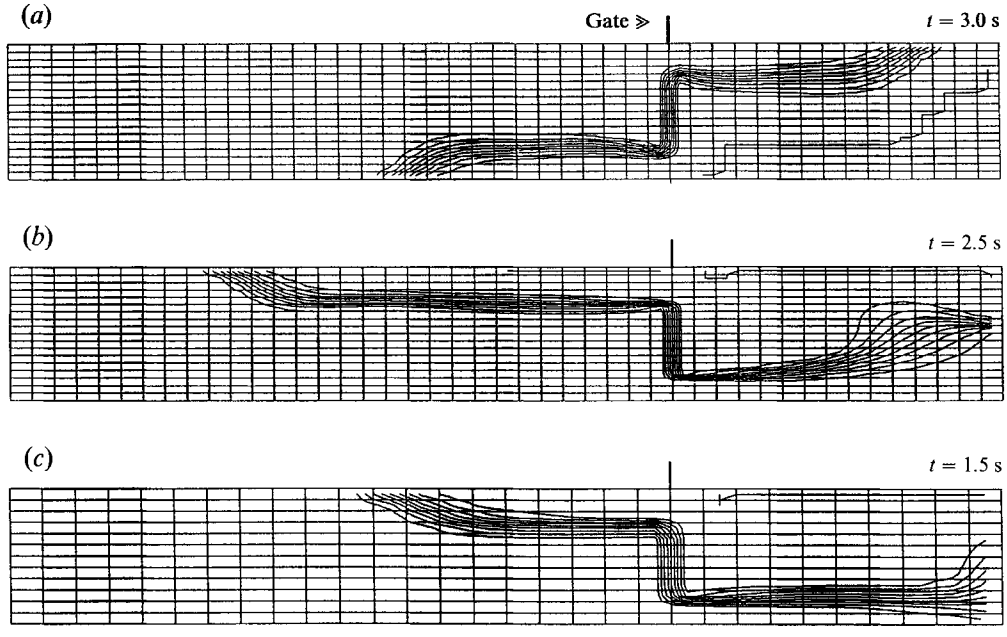

FIGURE 5. Isoconcentration lines for exchange flow: (*a*) argon in air, calculation grid, 45 × 18 cells; (*b*) helium in argon, calculation grid, 45 × 18 cells; (*c*) helium in R22, calculation grid, 30 × 12 cells.

5. Discussion

A compact form of representation is obtained when the velocity data, non-dimensionalized with $(gh)^{\frac{1}{2}}$, where $h = \frac{1}{2}H$, are plotted as a function of the density variable $\rho^* = [(\rho_2 - \rho_1)/(\rho_2 + \rho_1)]^{\frac{1}{2}}$ as shown in figures 6, 7 and 8. This representation is valid both in the weak (Boussinesq) and strong limit (cavity flow or zero counterpressure). The results obtained fall on two distinct curves: one representing the light-fluid fronts and the other the heavy-fluid fronts. Both branches coincide in the limit of vanishing density difference ($\rho^* = 0$).

For ease of reference, we have derived a relationship between Froude number $Fr = u_F/\sqrt{(gh)^{\frac{1}{2}}}$ and fractional depth $\Phi = h/H$ with the density variable ρ^* as parameter, in accord with Simpson (1987). By assuming horizontal flow and no pressure gradients or viscous drag, we obtain from continuity and the integral momentum balance the following relations:

$$Fr_H = \left[\left(\frac{1+\rho^{*2}}{1-\rho^{*2}} - 1\right)\frac{(2-\Phi)(1-\Phi)}{(1+\Phi)}\right]^{\frac{1}{2}} \quad \text{(heavy-fluid intrusion)}, \tag{7a}$$

$$Fr_L = \left[\left(1 - \frac{1-\rho^{*2}}{1+\rho^{*2}}\right)\frac{(2-\Phi)(1-\Phi)}{(1+\Phi)}\right]^{\frac{1}{2}} \quad \text{(light-fluid intrusion)}. \tag{7b}$$

We will first consider the results obtained for the lock-exchange experiments ($\Phi = \frac{1}{2}$). The representation Froude number $u_F/(gh)^{\frac{1}{2}}$ *vs.* ρ^* results in smooth curves over the full range of the density variable ρ^* as shown in figure 6(*a*). The lower branch (light-fluid intrusion) appears consistent with Benjamin's value in the limit of $\rho^* \to 1$, and the intermediate points moreover fall close to the predictions from (7*b*). The common slope for both branches for $\rho^* \to 0$ is in reasonable agreement with the theoretical value

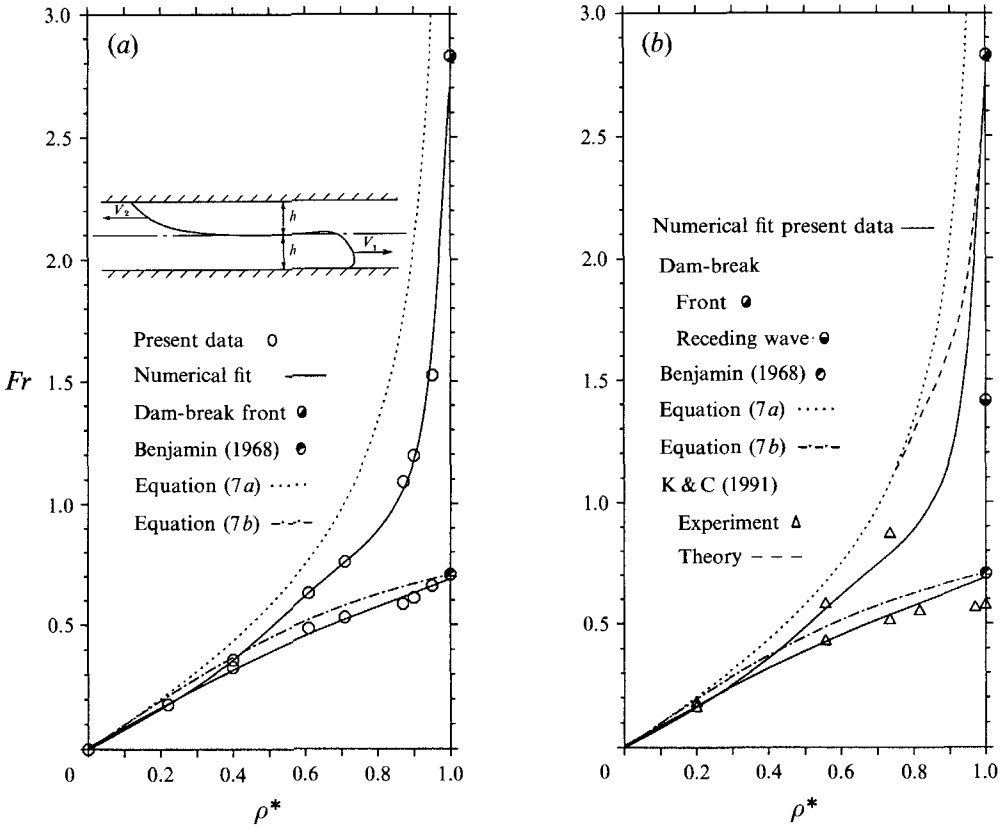

FIGURE 6. (*a*) Resulting Froude numbers of light- and dense-gas fronts for the complete range of density ratios. (*b*) Comparison of present data with theory and data from K & C. Lock-exchange flow, $\Phi = \frac{1}{2}$.

of 1 as predicted by Yih (1965). For the heavy-fluid intrusion, the Froude number limit as $\rho^* \to 1$ is not obvious. We have chosen for our fit to use the limit for the dam-break problem, i.e. $Fr = 2\sqrt{2}$ (Stoker 1957 or Henderson 1966). This solution is obtained from the shallow-layer equations and the receiving medium has unlimited depth. While perhaps not quite correct, the value $2\sqrt{2}$ comes close to what appears to be the best value, as will be seen later. A theory based on the balance of the hydrostatic pressure difference and the external drag predicts an infinite Froude number for strong dense fronts, (7*a*). But for such flows the wave velocity in the dense layer becomes the relevant parameter, as already noted.

Figure 6(*b*) shows data and a theoretical prediction for (part of) the strong branch published by K & C. Only for small to moderate density ratios do their values come close to our results as represented by the numerical fit. For density ratios near the strong limit, their results for the light-fluid intrusion fall about 15% below our values and the theoretical (Benjamin) limit. K & C give no experimental values for heavy-fluid fronts near the limit $\rho^* \to 1$, but a theoretical curve can be derived from the charts in their paper. In the intermediate range of ρ^*, this theory predicts much higher velocities than those measured. K & C's theory for strong gravity currents and the dam-break theory are closely related. Both are based on the shallow-layer equations, and the strong front has zero height in both models. This front is connected with the receding flow through a region of expansion waves and increasing flow depth. For the dam-

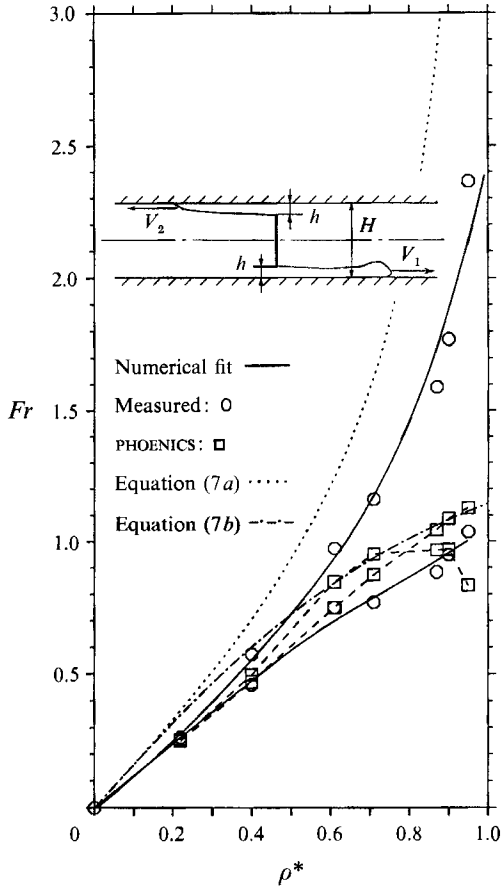

FIGURE 7. Comparison of calculated results with the measured data for exchange flow, $\Phi = \frac{1}{6}$.

break problem, the expansion region reaches all the way to the free surface (here, the top of the channel) whereas K & C argue that the receding flow is a cavity flow. By matching the wave region with Benjamin's solution, they obtain in the strong limit the value $Fr = 2.707$, only slightly below the value for the dam-break problem as indicated in figure 6(*b*). At intermediate density ratios, the results follow (7*a*) for $\rho^* < 0.749$. Our visualization (figure 3*c*), gives support to K & C's assumption that in the strong limit the receding flow is a Benjamin cavity and not a simple expansion wave. The velocity of the receding wave (dam-break) is twice the value calculated from (7*b*) and measured in the limit $\rho^* \to 1$ for the light-fluid intrusion. But this is true only for lock-exchange flows. In a medium of infinite depth, the dam-break problem appears to give the correct solution for both branches in the limit $\rho^* \to 1$.

For further support of this view, we turn to the results for the second experiment, an exchange flow of fractional depth $\Phi = \frac{1}{6}$. The experimental results and a numerical fit are shown in figure 7. The velocities are seen to be higher, as expected, and the experimental scatter more pronounced, than in the case of the lock-exchange problem, figure 6(*a*). Also included in figure 7, are the calculated results from the PHOENICS code. Quite consistent results are obtained over the full range of density ratios for the light-gas intrusion, whereas for $\rho^* > 0.6$ a breakdown appears to occur for the strong branch. The accuracy and validity of the code in the range considered is supported by

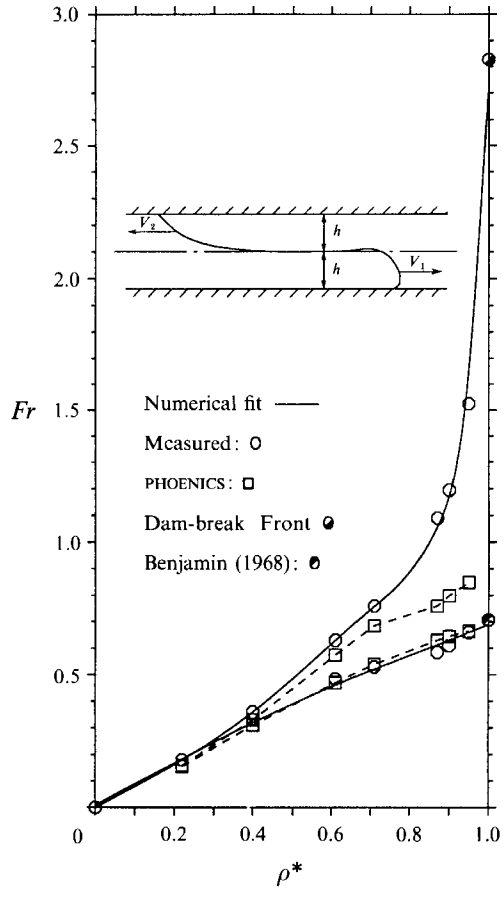

FIGURE 8. Comparison of calculated results with the measured data for lock-exchange flow, $\Phi = \frac{1}{2}$.

the results obtained for the lock-exchange problem, figure 8, at the least for the light-gas intrusions.

One hoped for end use of the exchange-flow results would be as an aid in the extrapolation from finite ($\Phi = \frac{1}{2}$, $\Phi = \frac{1}{6}$) to zero fractional depth. In figure 9 we have plotted the non-dimensional frontal velocity, for light- as well as heavy-gas intrusions, in terms of fractional depth $\Phi = h/H$. We have included the known limits of interest: Benjamin's value for $\Phi = \frac{1}{2}$; and for $\Phi = 0$ and, for the dam-break problem, the velocities of the front and the receding wave. It is difficult to label the closely spaced data points in figure 9 and for ease of interpretation the values are also tabulated in table 2.

The straight-line extrapolation for our highest density ratio (R22 in helium) gives a value only slightly below the analytical value for the dam-break problem. This is somewhat surprising as it is known that the limit velocity of this front of zero height, is considerably reduced when friction is taken into account (Dressler 1952). (But we note that the limit $\Phi = 0$ can be interpreted in two different ways. For the dam-break problem, the depth of the dam is finite and the front has zero height. For a heavy-gas intrusion, the front has finite height but the receiving medium is of infinite depth.) The scatter introduces some uncertainty in the extrapolated results. For the three cases, argon in CO_2, helium in R22 and R22 in helium, extrapolations according to (7*a*, *b*)

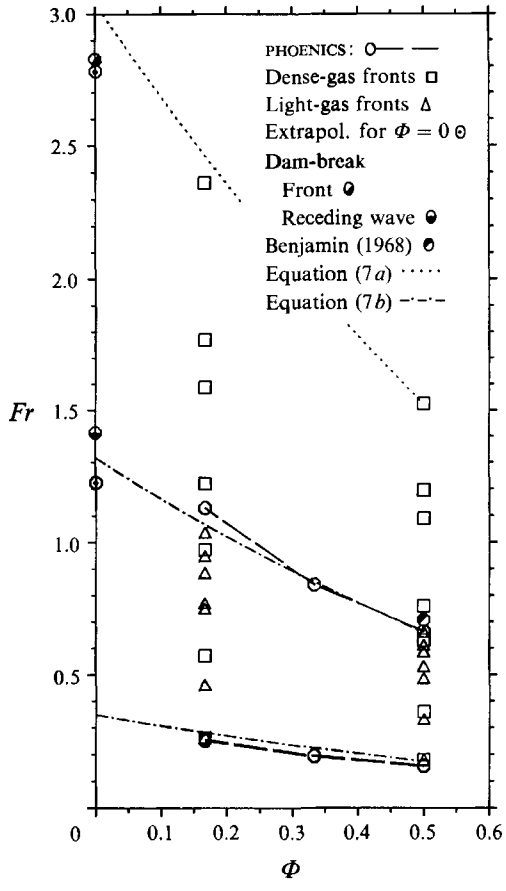

FIGURE 9. Froude number as function of fractional depth Φ (numerical values in table 2).

	Dense-gas fronts						Light-gas fronts					
	Measured		Extrap.	PHOENICS			Measured		Extrap.	PHOENICS		
Φ	$\frac{1}{2}$	$\frac{1}{6}$	0	$\frac{1}{2}$	$\frac{1}{3}$	$\frac{1}{6}$	$\frac{1}{2}$	$\frac{1}{6}$	0	$\frac{1}{2}$	$\frac{1}{3}$	$\frac{1}{6}$
ρ^*												
0.22	0.18	0.26	0.30	0.16	0.20	0.26	0.18	0.26	0.30	0.16	0.19	0.25
0.40	0.36	0.57	0.68	0.33	—	0.50	0.33	0.46	0.53	0.31	—	0.47
0.61	0.63	0.97	1.15	0.58	—	0.85	0.48	0.75	0.88	0.47	—	0.75
0.71	0.76	1.22	1.45	0.69	—	0.95	0.53	0.77	0.89	0.54	—	0.87
0.87	1.09	1.59	1.84	0.76	—	0.97	0.58	0.88	1.03	0.63	0.78	1.05
0.90	1.19	1.77	2.06	0.80	—	0.97	0.61	0.95	1.12	0.64	—	1.09
0.95	1.52	2.36	2.78	0.85	—	0.83	0.66	1.04	1.22	0.66	0.84	1.13

TABLE 2. Measured, extrapolated and calculated Froude numbers as function of fractional depth Φ and density parameter ρ^*. (A graphical representation is given in figure 9.)

are also indicated. The curves are adjusted with a reduced ρ^* in order to fit the measured values for $\Phi = \frac{1}{2}$. The corresponding values for $\Phi = \frac{1}{6}$ fall somewhat below the adjusted theoretical curve due to the greater importance of friction in the exchange-flow experiment. The simplifying assumptions used in deriving (7*a*, *b*) could also be

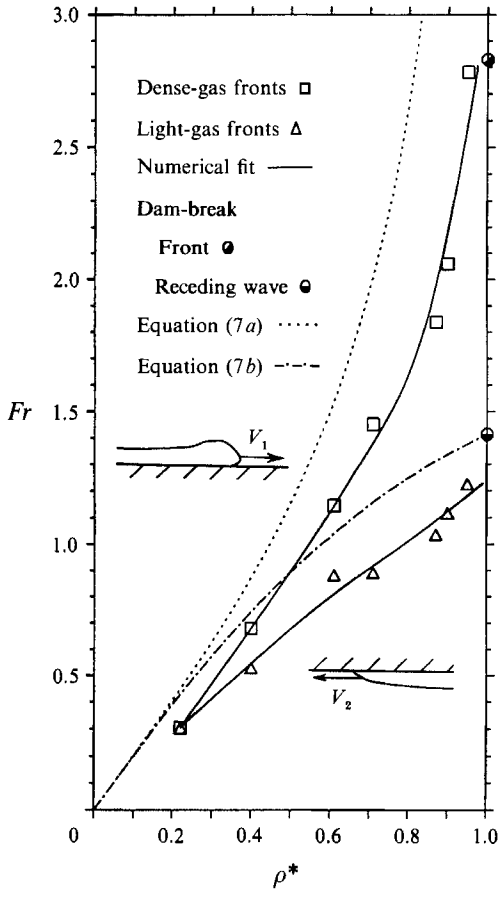

FIGURE 10. Extrapolated Froude number as function of ρ^* for $\Phi = 0$.

restrictive. For this reason a straight-line extrapolation from $\Phi = \frac{1}{2}$ and $\Phi = \frac{1}{6}$ to $\Phi = 0$ has been chosen. To check on the linearity of the $Fr(\Phi)$-curves, it was attempted to obtain 'exact' intermediate values of $\Phi(\Phi = \frac{1}{2}, \Phi = \frac{1}{3}, \Phi = \frac{1}{6}$ and $\Phi = \frac{1}{20})$ by means of the PHOENICS code. The calculation for $\Phi = \frac{1}{20}$ did not converge and the results for $\Phi = \frac{1}{6}$ appeared not fully reliable. Overall, the calculation indicated a weak curvature in $Fr(\Phi)$ as seen in figure 9 for the cases helium in R22 and argon in CO_2.

Figure 10 shows the tentative results of the extrapolations for $\Phi = 0$, based on our experimental results. The curve fits of the extrapolated data indicate that in the strong limit the dense-gas Froude number approaches the dam-break value. It also appears that the velocity of the receding wave represents an upper limit for light-gas fronts of high density ratio in a medium of unbounded depth. A description of the flow based on shallow-layer theory appears to be in reasonable agreement with the data. For small ρ^* both branches coincide near the origin with a slope of about 2, which is the predicted value for a weak front ((1 *a*, *b*) with $k = \sqrt{2}$).

6. Conclusions

The results obtained show that gravity fronts of high density ratio differ considerably in speed of propagation and shape in comparison with the more familiar (Boussinesq) fronts with density ratio close to unity. The representation of Froude number, $u_F/(gh)^{\frac{1}{2}}$,

vs. the density parameter $\rho^* = [(\rho_2 - \rho_1)/(\rho_2 + \rho_1)]^{\frac{1}{2}}$, gives well-defined curves over the complete range of density ratios for both the heavy- and the light-fluid fronts. The rather large difference in speed of propagation between these configurations, at all fractional depths investigated, appears to be a new result not recognized in two important applications: fire research and the dispersion of dense (hazardous) chemicals. For lock-exchange flows, our results for the light-fluid intrusion agree at one end of the range ($\rho^* = 1$) with Benjamin's result for the propagation of a cavity and at the other ($\rho^* = 0$) with the known value for small density differences. In between, our data agree well with results predicted from integral continuity and momentum balances. The heavy-fluid fronts can be predicted only for low to moderate density ratios.

The results for small fractional depths ($\Phi = \frac{1}{6}$) are similar to those for the lock-exchange case. Different curves are again observed for the light- and heavy-fluid fronts. Both experimental and numerical results (from the PHOENICS code) have been utilized in our extrapolation to the case of infinite depth, $\Phi \to 0$. This is the case most likely to be of interest in practical applications. In comparison with the known limits, the extrapolated values appear somewhat too low, most likely related to viscous effects affecting primarily the case $\Phi = \frac{1}{6}$. The extrapolation amplifies the errors in the measured values. The results obtained in the double limit $\Phi \to 0$ and $\rho^* \to 1$ indicate a limit speed of propagation equal to that predicted based on shallow-layer theory (dam-break), i.e. $Fr = 2\sqrt{2}$ for the heavy-fluid front and $Fr = \sqrt{2}$ (receding wave) for the light-fluid front.

The fundamental differences between the light- and heavy-fluid intrusions are confirmed by our visualization studies. The light-fluid front is elongated, smooth and generally loss free with a contour in agreement with Benjamin's (1968) ideal theory. The heavy-fluid front is blunt and gives more evidence of mixing and other loss processes (hydraulic jumps).

Certain parts of this work were undertaken as student projects in the period October 1989 to December 1991. The experimental set-up was assembled by Dipl.-Ing. E. Lutz and Dipl.-Ing. I. Martin. Dipl.-Ing. S. Lamprecht helped develop the flow visualization system and carried out certain exchange-flow experiments including observations of the height of the intruding layers. The influence of gate opening time was investigated by Ing. ETH A. Gamboa.

REFERENCES

BATILL, S. M., MUELLER, T. J. 1981 Visualization of transition in the flow over an airfoil using the smoke-wire technique. *AIAA J.* **19**, 340.

BENJAMIN, T. B. 1968 Gravity currents and related phenomena. *J. Fluid Mech.* **31**, 209.

BRITTER, R. E. 1989 Atmospheric dispersion of dense gases. *Ann. Rev. Fluid Mech.* **21**, 317.

DRESSLER, R. F. 1952 Hydraulic resistance effect upon the dam-break functions. *J. Res. Natl Bur. Stand.* **49**, 217.

FANNELØP, T. K. & JACOBSEN, Ø. 1983 Experimental and theoretical studies in heavy gas dispersion. In *Atmospheric Dispersion of Heavy Gases and Small Particles* (ed. G. Ooms & H. Tennekes). Springer.

FANNELØP, T. K. & WALDMAN, G. D. 1971 Dynamics of oil slicks. *AIAA J.* **10**, 506.

FAY, J. A. 1969 The spread of oil on a calm sea. In *Oil on the Sea.* Plenum.

FAY, J. A. 1982 Some unresolved problems of LNG vapor dispersion. *MIT-GRI, LNG Safety and Research Workshop.* Gas Research Institute, Chicago.

HENDERSON, F. M. 1966 *Open Channel Flow.* Macmillan.

KARMAN, T. VON 1940 The engineer grapples with nonlinear problems. *Bull. Am. Math. Soc.* **46**, 615.

KELLER, J. J. & CHYOU, Y.-P. 1991 On the hydraulic lock-exchange problem. *Z. Angew. Math. Phys.* **42**, 874 (referred to herein as K & C).

KUNSCH, J. P., GRÖBELBAUER, H. P., BILLETER, L. & FANNELØP, T. K. 1991 Schwergasforschung an der ETH-Zürich Beitrag zum IV. *Symp. on Schwere Gase und Sicherheitsanalyse Bonn, 26./27. September 1991.*

LAMB, H. 1945 *Hydrodynamics*, 6th edn. Dover.

MCQUAID, J. 1985 Objectives and design of the Phase I Heavy Gas Dispersion Trial. *J. Haz. Mat.* **11**, 1.

ROSTEN, H. I., SPALDING, D. B. 1987 *The PHOENICS Reference Manual.* Wimbledon: CHAM Ltd.

SIMPSON, J. E. 1987 *Gravity Currents, in the Environment and the Laboratory.* Ellis Horwood.

STOKER, J. J. 1957 *Water Waves.* Interscience.

YIH, C-S. 1965 *Dynamics of Nonhomogeneous Fluids.* Macmillan.